Electronic Supplementary Material (ESI) for CrystEngComm.
This journal is © The Royal Society of Chemistry 2015

Supplementary Information

Reliable Palladium Nanoparticle Syntheses in Aqueous Solution: The Importance of Understanding Precursor Chemistry and Growth Mechanism

Frieder Kettemann[a], Maria Wuithschick[a], Gianvito Caputo[a], Ralph Kraehnert[b], Nicola Pinna[a], Klaus Rademann[a], and Jörg Polte*[a]

[a] Humboldt-Universität zu Berlin, Department of Chemistry, Brook-Taylor-Strasse 2, 12489 Berlin, Germany
[b] Technische Universität Berlin, Technische Chemie, Strasse des 17 Juni 124, 10623 Berlin, Germany

Contents

S1. Experimental details
S2. Hydrolysis of Pd complexes in aqueous solutions
S2.1 Time-resolved UV-vis of K_2PdCl_4 aging
S2.2 Time-resolved UV-vis of Na_2PdCl_4 aging
S2.3 Time-resolved UV-vis of $Pd(NO_3)_2$ aging
S2.4 Time-resolved SAXS data of K_2PdCl_4 aging
S2.5 Time-resolved SAXS data of $Pd(NO_3)_2$ aging
S2.6 XRD data of Pd hydrolysis products
S3. NP synthesis with aged and pH-stabilized precursor solutions
S4 TEM images of Pd-NPs
S5. Large-scale synthesis of Pd-NPs
S6. Experimental setups
S6.1 Continuous flow setup (CFS)
S6.2 Large-scale synthesis of Pd-NPs
S7 Influence of mixing conditions on the NP size
S8 Evaluation of SAXS data

S1 Experimental details

All chemicals were used as received without any further purification. Ultrapure water (18.2 MΩ·cm, Millipore) was used as solvent for all reactions.

Table 1: List of used chemicals

Compound	Purity	Supplier
K_2PdCl_4	99.999%	Alfa Aesar
$Pd(NO_3)_2$		Sigma Aldrich
Na_2PdCl_4	99.999%	Alfa Aesar
$NaBH_4$ (granulate)	99,99%	Sigma Aldrich
NaOH	p.a.	Carl Roth
$HClO_4$	99.99%	Sigma Aldrich
Polyvinylpyrrolidone (PVP) MW 58,000		Alfa Aesar

Synthesis of Pd-NPs: A 3 mM $NaBH_4$ solution was prepared by dissolving 113.5 mg of $NaBH_4$ (Sigma Aldrich 99,99%) in 1 l of ultrapure water (18.2 MΩ·cm, Millipore). For each experiment the $NaBH_4$ solution was freshly prepared and used within1 min after dissolving. The precursor solutions were prepared by dissolving 8.16 mg of K_2PdCl_4 (99.999%, Alfa Aesar) in 50 ml of Milli-Q water to give a 0.5 mM solution. For the preparation of precursor solutions with a certain pH value the appropriate amount of precursor salt was dissolved in a solution of diluted NaOH (p.a., Carl Roth) or $HClO_4$ (99.99%, Sigma Aldrich). The pH value of the NaOH or $HClO_4$ solution was adjusted with a pH-electrode (Mettler Toledo).
For the synthesis of Pd-NPs 5 ml of a freshly prepared 3 mM $NaBH_4$ solution was mixed 1:1 with 5 ml of a 0.5 mM solution of K_2PdCl_4 with a pH value of 3.3 using Eppendorf pipettes. The reaction mixture was continuously stirred with a teflon bar exactly fitting the sample glass (borosilicate 3.3, Carl Roth) at 300 rpm.

Characterisation:
UV-Vis spectra of the precursor solutions were measured with a SEC2000 spectrometer (BAS Inc.) using PMMA cuvettes.
SAXS experiments were carried out on a lab-scale setup (SAXSess, Anton Paar using a flow through quarts cuvette (Anton Paar).
TEM: Transition Electron Microscopy (TEM) analysis was carried out using a CM200 LaB_6 Philips microscope operated at 200 kV. A few drops of a Pd-NP solution were deposited on a copper grid coated with an amorphous carbon film and dried in air.

S2. Hydrolysis of Pd complexes in aqueous solutions

$Pd(NO_3)_2$, Na_2PdCl_4 and K_2PdCl_4 are highly soluble in water giving transparent yellow solutions. Within minutes the color of aqueous Pd solutions changes successively from yellow to brown. For tetrachloropalladates the solution becomes turbid and after approx. 7 hours precipitation is observed (see Figure S1)

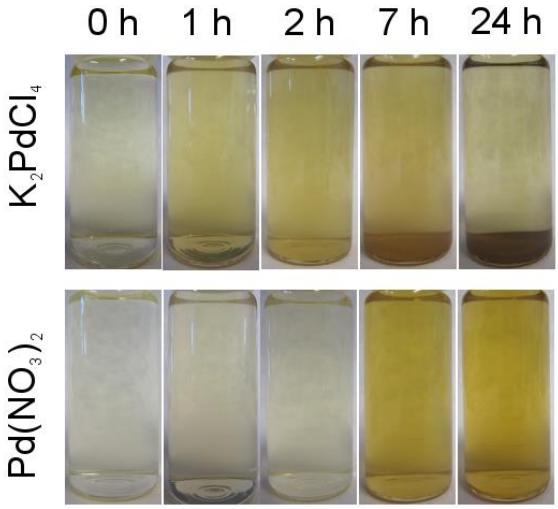

Figure S1: Photographs of aging a 1 mM K_2PdCl_4 and $Pd(NO_3)_2$ solution.

Pd complexes hydrolyze in aqueous solution.[1] The formed Pd aquo complexes readily undergo olation to give polynuclear hydroxo complexes (PHC):[2]

$$[Pd(H_2O)_4]^{2+} \rightarrow [Pd(OH)_4]^{2-} + 4\,H^+$$

$$n[Pd(OH)_4]^{2-} \rightarrow [Pd(OH)_2]_n + 2n\,OH^-$$

These PHC are subject to further oxolation and precipitation of PdO like structures is observed (see S2.6 for XRD data).

The kinetics of this process can be easily monitored by UV-vis spectroscopy. A broad increase in absorbance accompanies with formation of PHC.[3] The hydrolysis of Pd complexes and the formation of PHC are strongly dependent on the pH value. Thus, aging of aqueous Pd solutions was investigated with UV-vis spectroscopy at different pH values (see S2.1-S2.3). The absorbance at the respective maxima is plotted against aging time. Low pH values decelerate the formation of PHC. At pH values < 2 the formation of PHC is not observed within 50 min. In contrast, basic conditions accelerate the formation of PHC since the exchange of water molecules by hydroxide anions is promoted.

Additionally to UV-vis measurements, time-resolved SAXS measurements were performed (see S2.4 and S2.5). The data indicate that for both, solutions (K_2PdCl_4 and $Pd(NO_3)_2$), PHC are formed within minutes for neutral and basic solutions. The formation of PHC is decelerated for acidic conditions. Scattering of colloidal PHC is not observed for very acidic solutions (pH<2,5) for hours. For solutions with a pH value of 3.3 the formation of PHC is not observed after 3 h for K_2PdCl_4 solutions. In $Pd(NO_3)_2$ solutions with a pH value of 3.3 slight formation of colloidal PHC is observed after approx. 30 min.

Cl^- ions seem to play a crucial role for the size of the PHC. Within hours visible micro particles are formed in $PdCl_4^{2-}$ solutions. Precipitation is not observed for solutions that

do not contain Cl^- (like $Pd(NO_3)_2$) within months. The addition of Cl^- to a $Pd(NO_3)_2$ solution results in precipitation of PHC within hours. Troitskii et al. showed that in precipitated PHC from $PdCl_4^{2-}$ solutions, Cl^- remains in the PHC precipitate.[2] Cl^- as a bridging ligand could induce further growth of PHC until they reach a size that leads to precipitation. In the absence of Cl^- the growth of PHC stops if the PHC colloids reach a stable size.

S2.1 Time-resolved UV-vis of K_2PdCl_4 aging

The results of time-resolved UV-vis measurements of precursor aging at different pH values are displayed in Fig. S2. A broad increase in absorbance evolves within seconds, due to formation of PHC. Higher pH values accelerate the formation of PHC. At pH values of 2, the formation of PHC is not observed.

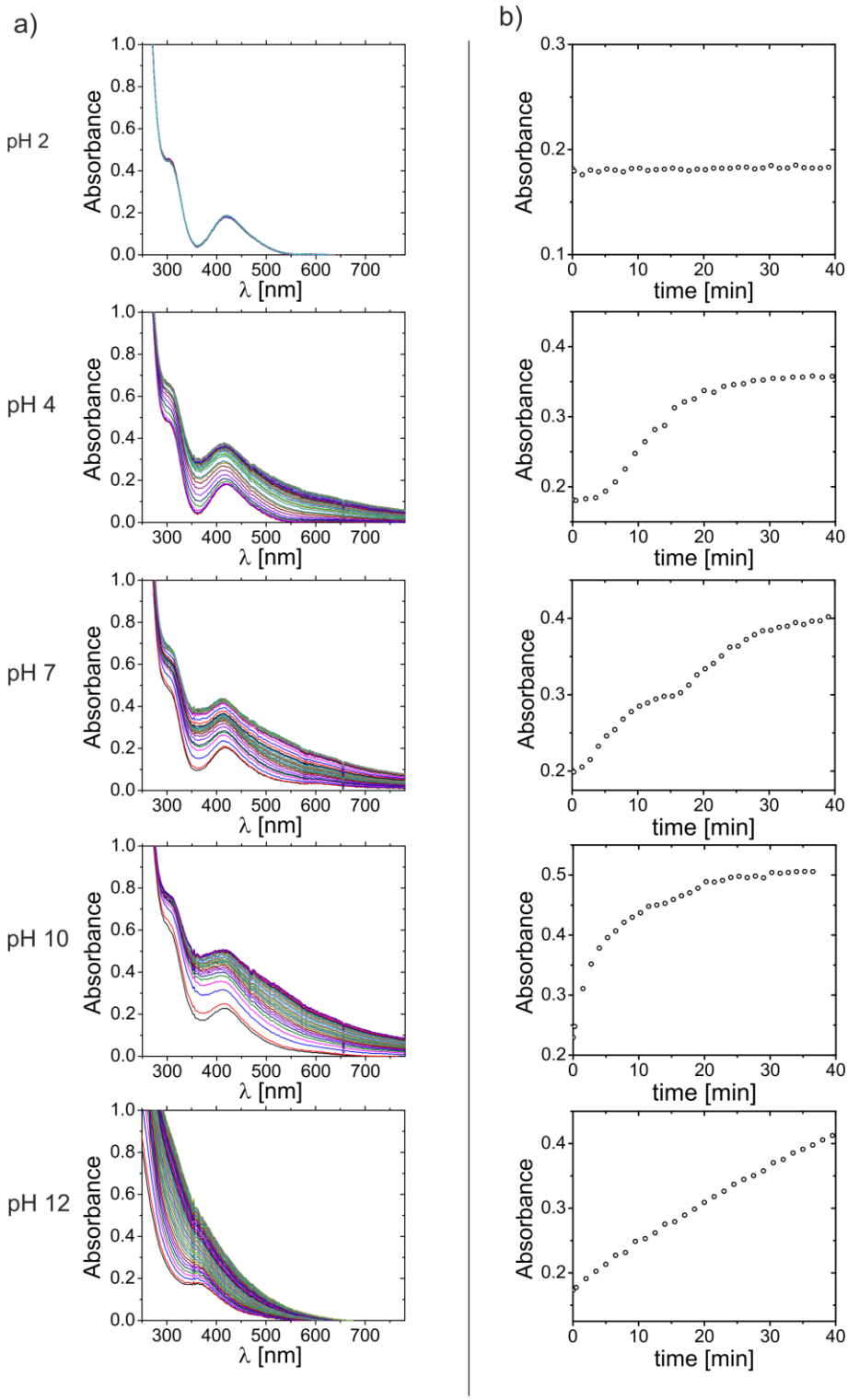

Figure S2: (a) Time-resolved UV-vis data for the aging of a 1 mM K_2PdCl_4 solution at different pH values; (b) the absorbance at 420 nm (370 nm for pH 12) is plotted against the aging time.

S2.2 Time-resolved UV-vis of Na_2PdCl_4 aging

The time-resolved UV-vis measurements of Na_2PdCl_4 aging in aqueous solution (Fig. S3) show a similar behavior as K_2PdCl_4 solutions (see S2.1). This indicates that the cation has no influence on the precursor aging.

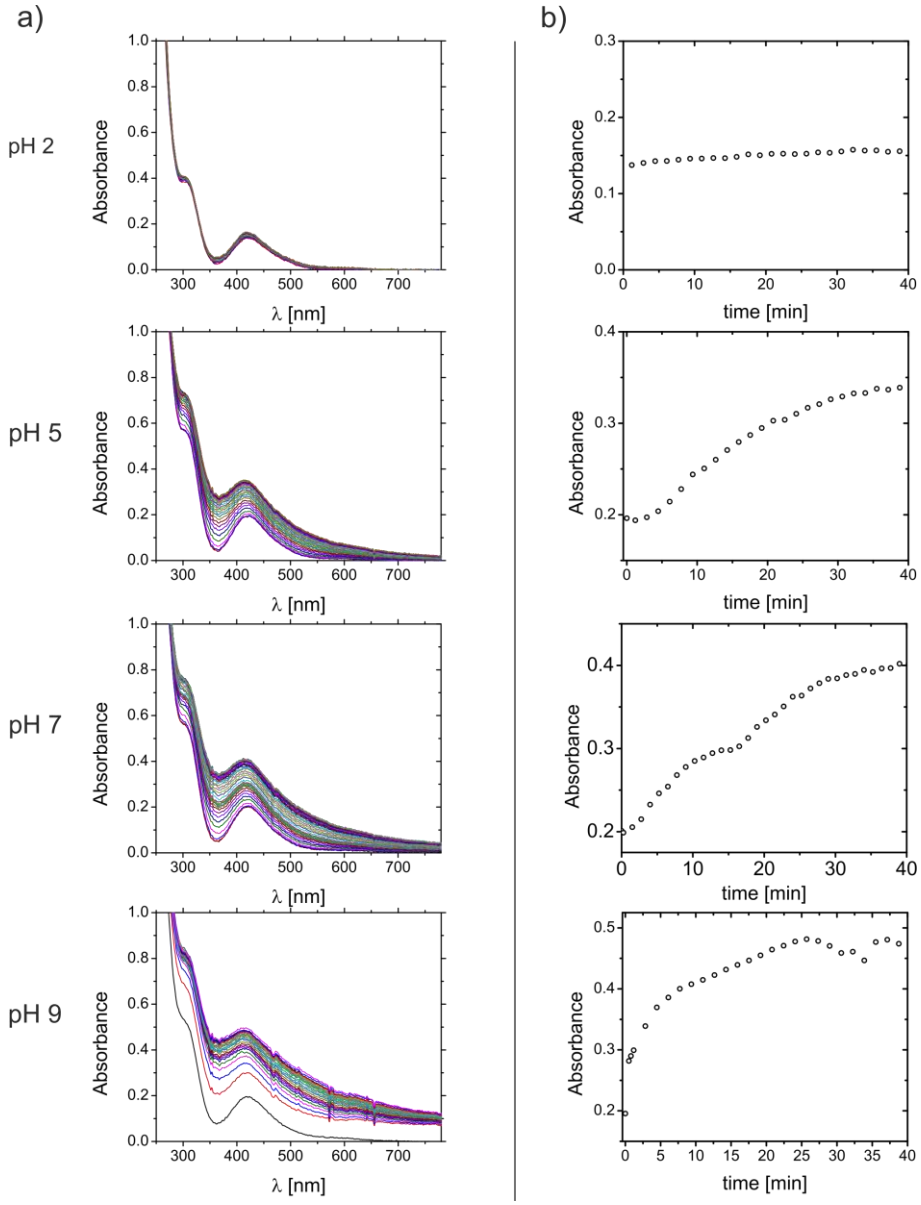

Figure S3: (a) Time-resolved UV-vis measurements for the aging of a 1 mM Na_2PdCl_4 different pH a value; (b) the absorbance at 420 nm is plotted against the aging time.

S2.3 Time-resolved UV-vis of $Pd(NO_3)_2$ aging

The results of time-resolved UV-vis measurements of $Pd(NO_3)_2$ aging in aqueous solution at different pH values are displayed in Fig. S4. A broad increase in absorbance is observed within seconds of the precursor dissolution, due to the formation of PHC. Higher pH values accelerate the formation of PHC. The UV-vis spectrum remains constant for strongly acidic conditions.

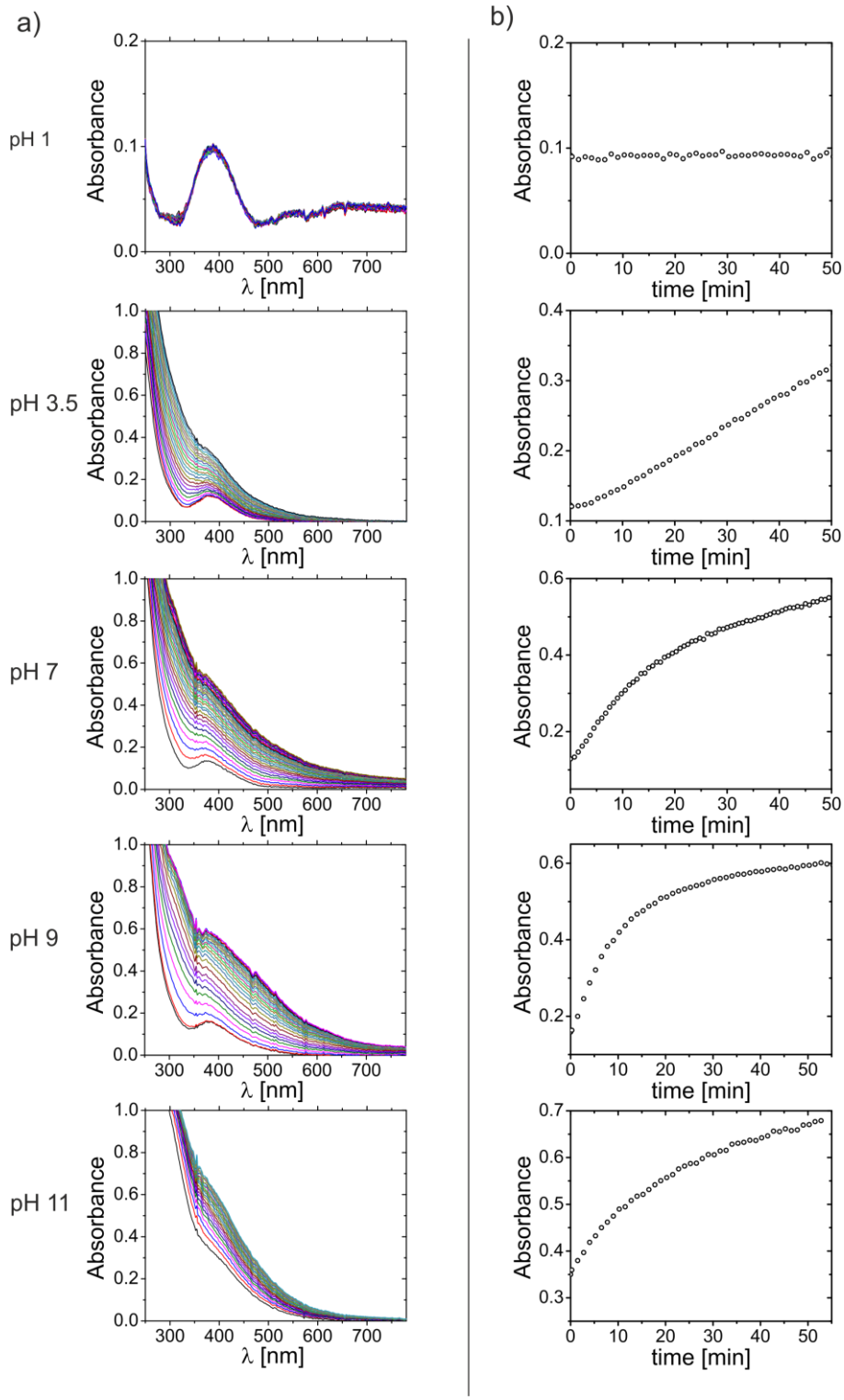

Figure S4: (a) Time-resolved UV-vis measurements for the aging of a 1 mM $Pd(NO_3)_2$ solution at different pH values; (b) the absorbance at 370 nm is plotted against the aging time.

S2.4 Time-resolved SAXS data of K_2PdCl_4 aging

Selected scattering curves for the aging of K_2PdCl_4 are displayed in Fig. S5. For very short aging times (30s) the formation of colloidal PHC is not observed and the scattering curves show only random noise. With increasing aging time, the scattering curves for K_2PdCl_4 solutions with a pH values < 3.3 show an increased intensity at lower q values. This is due to the formation of large structures which are most likely the PHC. In general, higher pH values accelerate the formation of PHC.

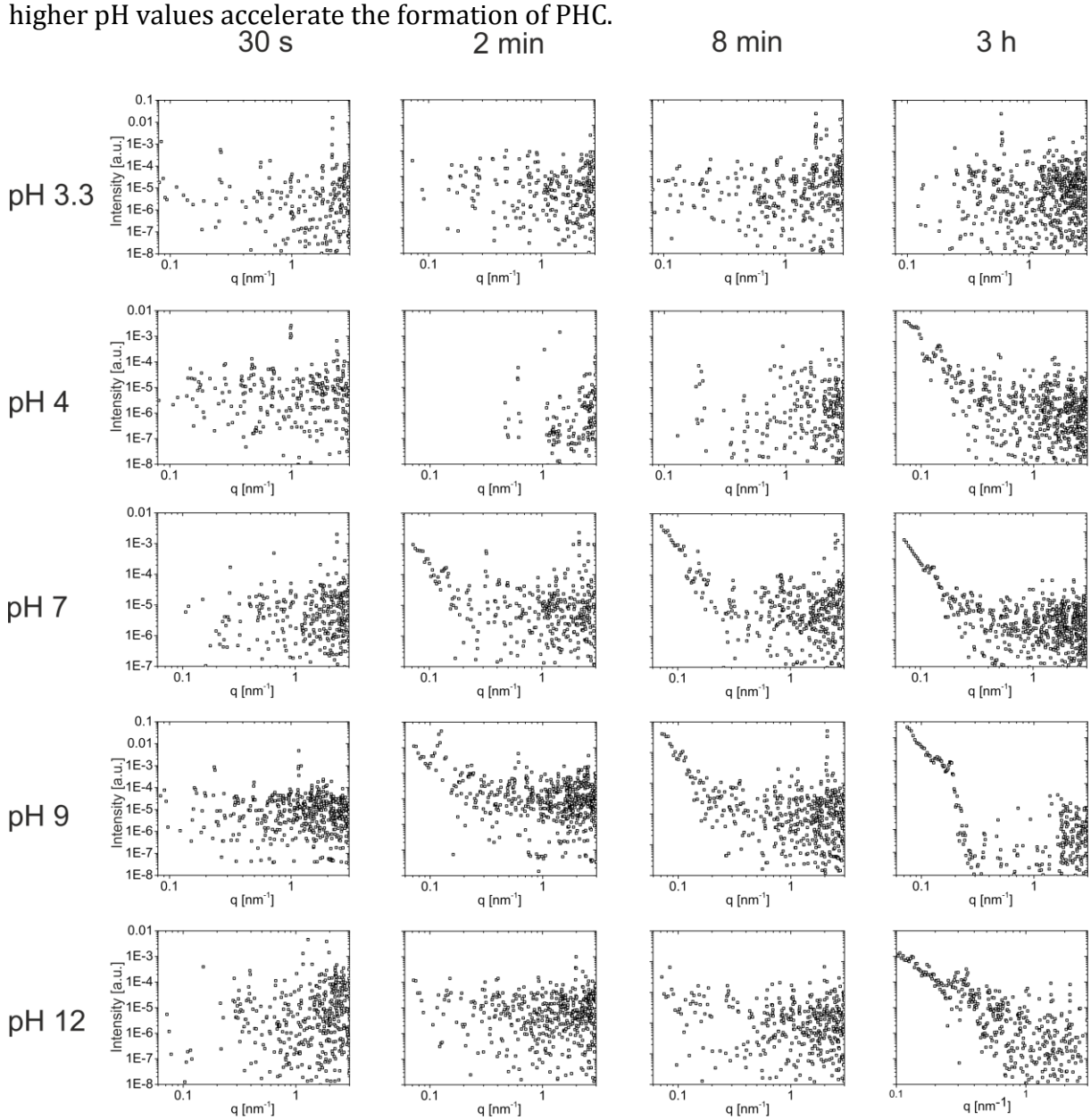

Figure S5: Scattering curves from time-resolved SAXS measurements for aging of a 0.5 mM K_2PdCl_4 solution.

S2.5 Time-resolved SAXS data of $Pd(NO_3)_2$ aging

Selected scattering curves for the aging of a 0.5 mM $Pd(NO_3)_2$ solution are displayed in Fig. S6. For very short aging times (30s) the formation of colloidal PHC is not observed for pH values of 9 or lower. The scattering curves show only random noise. With increasing aging time, the scattering curves for K_2PdCl_4 solutions with a pH values > 2 show an increased intensity at lower q values. This is due to the formation of large structures which are most likely the PHC. In general, higher pH values accelerate the formation of PHC.

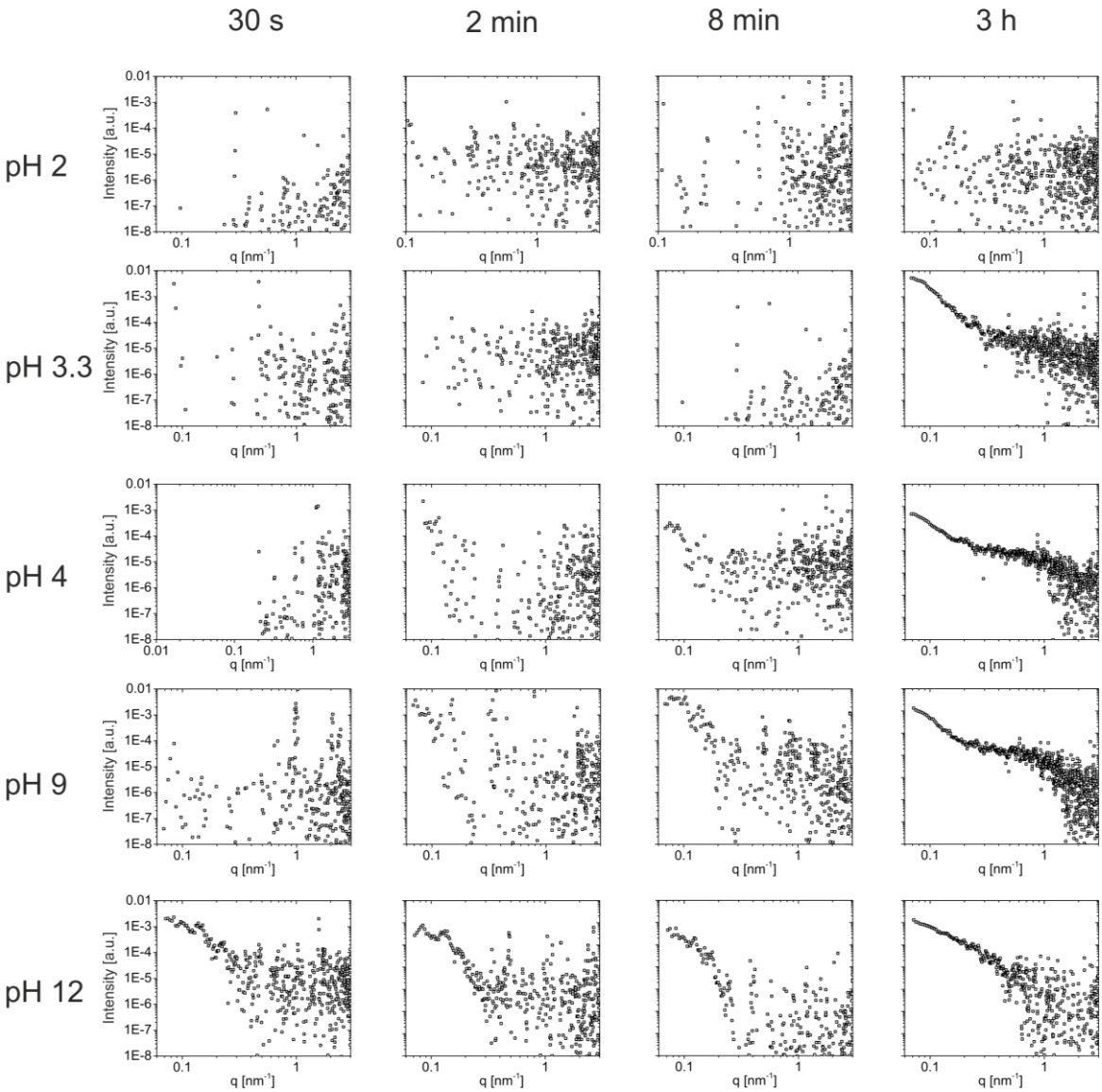

Figure S6: Scattering curves form time-resolved SAXS measurements foraging of a 0.5 mM $Pd(NO_3)_2$ solution at different pH values.

S2.6 XRD data of Pd hydrolysis products

XRD data (Fig. S7) of the precipitates from different aqueous Pd solutions show characteristic reflections at 34° and 55° that are typical for PdO.[4] The reflections at 34° are due to the formation of PdO like structures within the PHC.[3] Since precipitation is not observed for $Pd(NO_3)_2$ solutions, the solid was collected with centrifugal filters.

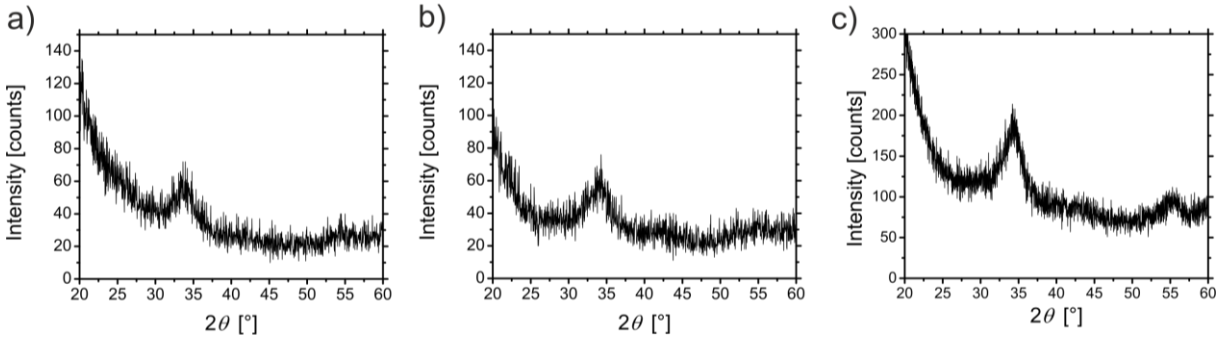

Figure S7: XRD data from the precipitate of aged precursor solutions (a) K_2PdCl_4; (b) Na_2PdCl_4; (c) $Pd(NO_3)_2$.

S3. NP synthesis with aged and stabilized precursor solutions

The reproducibility of the NP synthesis was investigated by performing the synthesis of Pd-NPs with non-pH-stabilized precursor solutions (aging time 6 min) and precursor solutions with a pH value of 3.3 (i.e. pH-stabilized precursor solutions) for three times. Two representative scattering curves of the final particles are displayed in Fig. S8.
NPs synthesized from a non-pH-stabilized precursor solution show a broad size distribution that cannot be fitted accurately. The scattering at low q values is due to larger structures. The scattering curves are fitted separately at high and low q values to estimate the size of the formed particles. NPs from stabilized precursor solutions have mean radii of approx. 2.3 nm with a relatively low polydispersity of 30%. The results of the reproducibility study are displayed in Table S2 and S3.

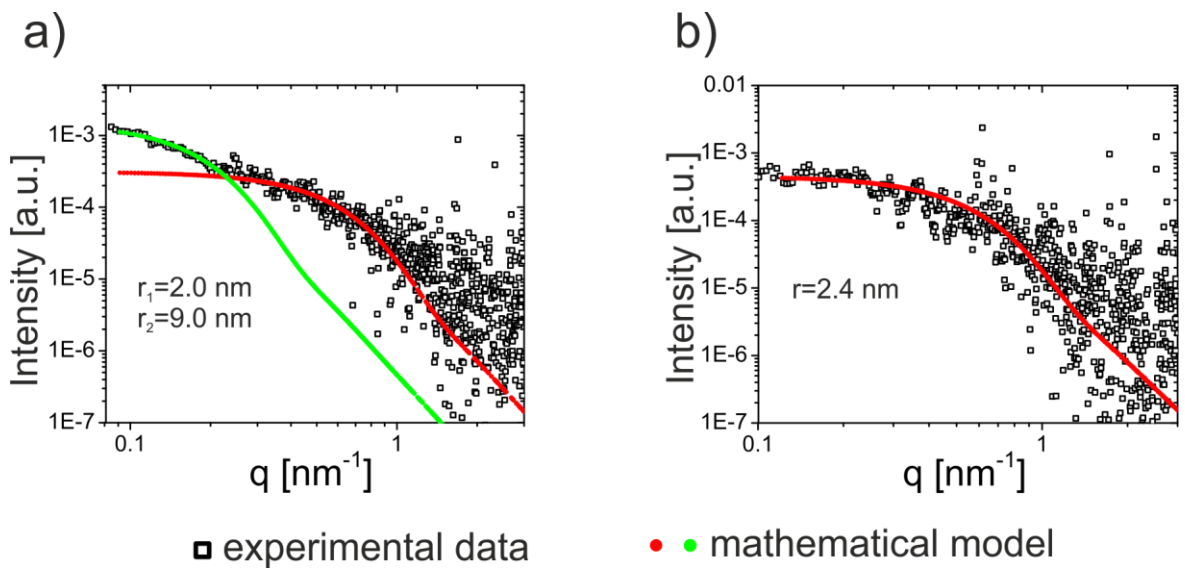

Figure S8: Scattering curves of NP synthesized from different 0.5 mM precursor solutions: (a) non-pH-stabilized K_2PdCl_4; (b) K_2PdCl_4 with a pH value of 3.3; the polydispersity is 30%.

Table S2: Mean radii of Pd-NPs synthesized with a K_2PdCl_4 solution that aged for 6 min; the scattering curves are fitted separately at higher and lower q values with a polydispersity of 30% to estimate the size distribution.

r small particles [nm]	r large particles [nm]
2.5	8.4
2.0	9.0
3.0	9.9

Table S3: Mean radii of NP synthesized from a K_2PdCl_4 solution with a pH value of 3.3.

radius [nm]	polydispersity
2.3	30%
2.4	30%
2.3	30%

S4. TEM images of Pd-NPs

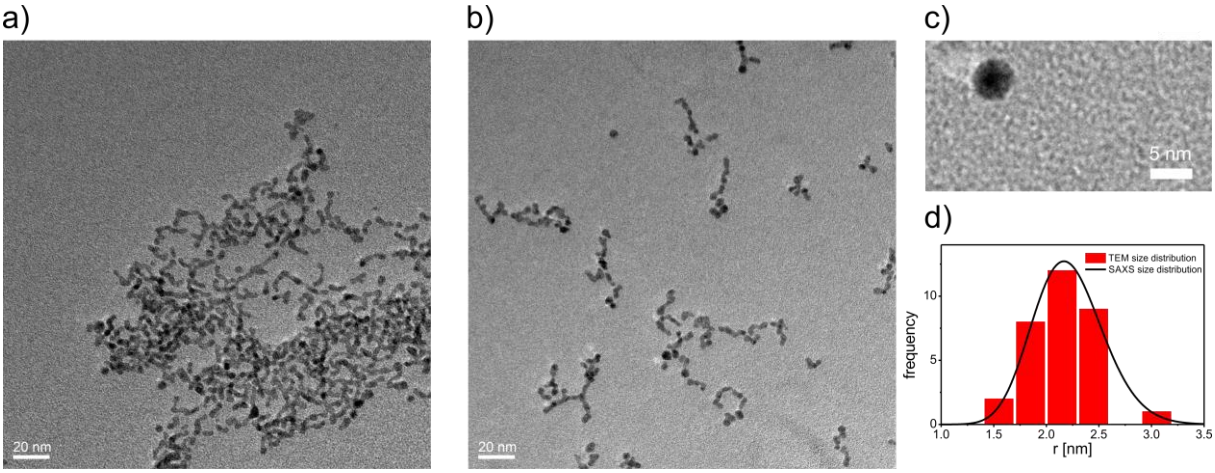

Figure S9: TEM images of final Pd-NPs prepared by the reduction of a pH-stabilized K_2PdCl_4 solution (pH 3.3); (a) as-prepared, (b) diluted 1:10; (c) individual Pd-NP; (d) histogram comparing particle size distribution measured by TEM and SAXS (cf. S3).

Figure S9 shows representative TEM images of Pd-NPs prepared with pH-stabilized precursor solution (pH 3.3). The as-prepared NPs show aggregation on the TEM grid (Fig. S9 a). The NP solution was diluted (1:10) to decrease particle aggregation on the grid (Fig. S9 b). However, aggregation remains an issue. The shape and exact size of the aggregated NPs are difficult to determine. Nevertheless, individual NPs on the grid can be investigated, as shown in Fig. S9 c. These are of spherical shape with a mean radius of 2.2 nm which is in good agreement with the corresponding SAXS data (see histogram in Fig. S9 d).

From the SAXS experiments it can be concluded that the observed aggregation on TEM grids does not represent the state in solution. Large aggregates scatter at low q-values ($q < 0.3\ nm^{-1}$). Such scattering intensity is not observed. Thus, the aggregation of the particles on the grid could be tentatively explained with the drying process.

S5. Large-scale synthesis of Pd-NPs

The large-scale synthesis of Pd-NPs was performed with a pH-neutral K_2PdCl_4 solution (non-pH-stabilized solution) and one with a pH value of 3.3 (pH-stabilized solution). Both solutions were freshly prepared. The reagents were mixed (1:1) with a peristaltic pump for 1 and 10 min, giving 500 ml of NP solution. A description of the experimental setup can be found in S5. The scattering curves of the resulting NP are displayed in Fig. S10. Already at a mixing time of 1 min, NP synthesized from non-pH-stabilized precursor solution show a broad size distribution. The increased intensity towards lower q values indicates the formation of larger particles. At a mixing time of 10 min the scattering curve reveals a very broad size distribution that cannot be fitted accurately. The increased intensity is due to scattering of large particles with radii of about 20 nm. The scattering at higher q values can be attributed to particles with radii of approx. 3nm. Particles from pH-stabilized precursor solutions have mean radii of 2.1 nm and a polydispersity of 25% for both mixing times. Selected scattering curves are displayed in Fig. S10.

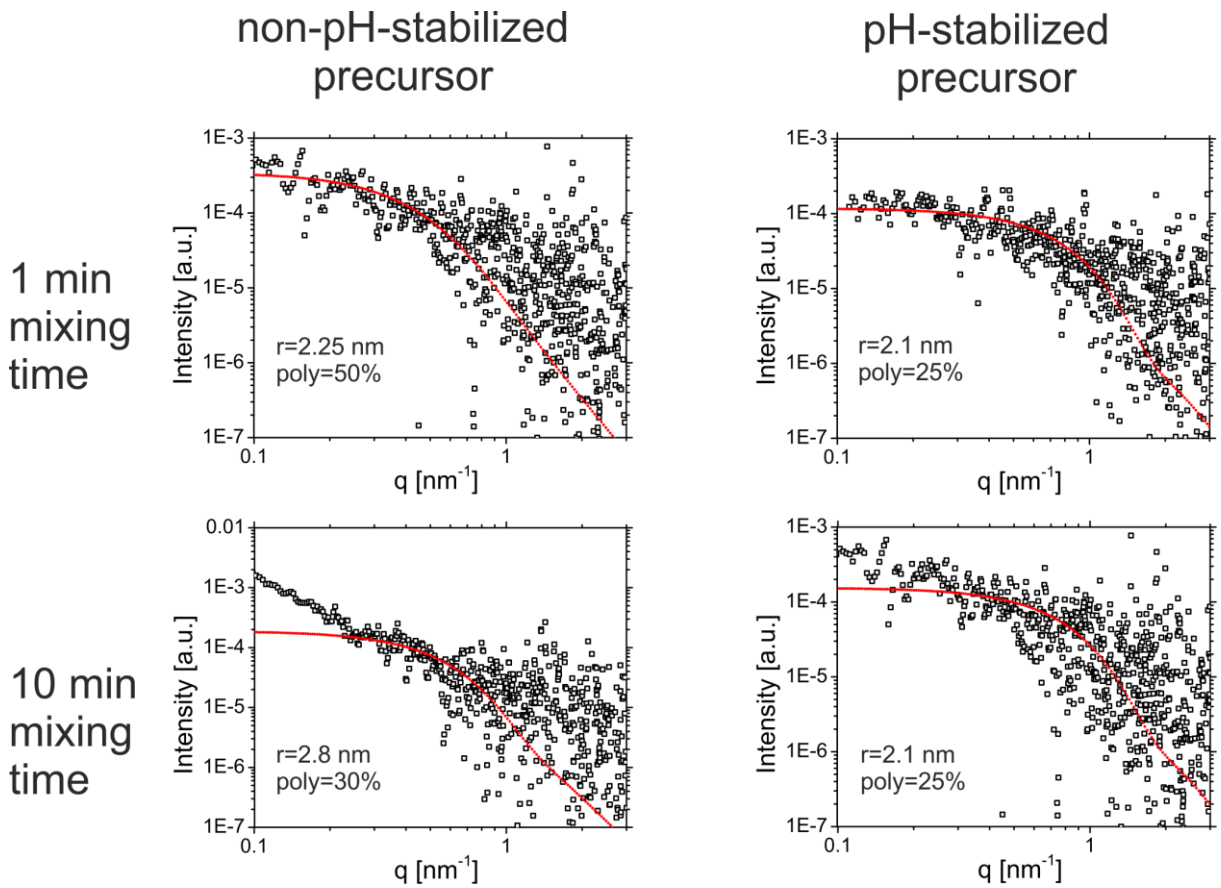

Figure S10: Scattering curves of NPs synthesized with the large-scale setup with mixing times of 1 and 10 min; non-pH-stabilized precursor solutions are neutral, while pH-stabilized precursor solutions have a pH value of 3.3.

S6. Experimental setups

S6.1 Continuous flow setup (CFS)

A typical SAXS measurement of colloidal NPs with a lab scale SAXS setup has a time resolution of around a minute or more. This is insufficient for the investigation of the NP growth in the first seconds. Thus, a continuous flow setup was applied in order to overcome the limited time-resolution. In a CFS, the time scale of a reaction is transformed into a length scale. This enables the investigation of the NP growth in the first milliseconds of the reaction.[5] The setup is schematically illustrated in Fig. S11.
A syringe pump was used to transport the reagents via Teflon tubings. The reactants were mixed in a Teflon Y-mixer. The reaction time was varied by adjusting the tube length (Δd) and diameter between the mixer and flow through quartz capillary (inner diameter of 1 mm and wall thickness of 10 µm, Anton Paar, Graz, Austria). The time delay between mixing and measurement corresponds to the reaction time (Δt).

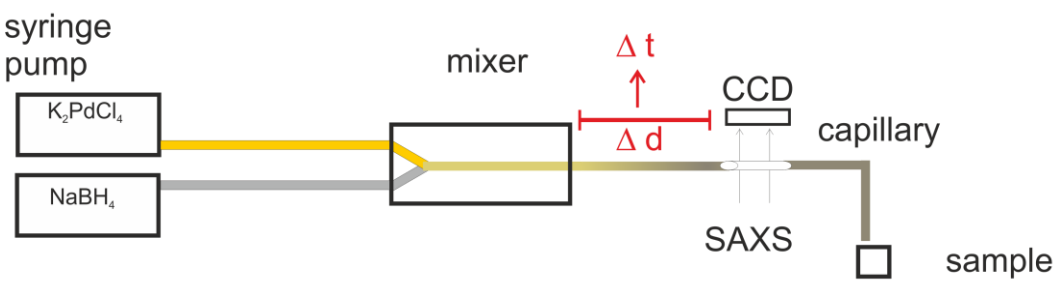

Figure S9: Schematic illustration of the continuous flow setup (CFS).

S6.2 Large-scale synthesis of Pd-NPs

For the large scale synthesis of Pd-NPs, a peristaltic pump (Watson Marlow) was used to mix the precursor solution and $NaBH_4$ solution via Teflon tubes and a Teflon mixer. The setup is schematically displayed in Fig. 12. The mixing time of the reagents was varied by adjusting the flow rate of the peristaltic pump.

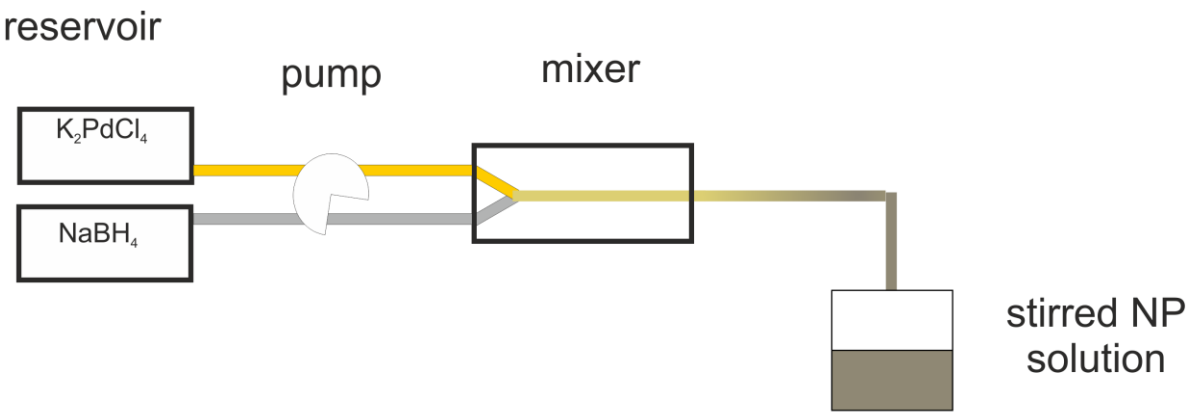

Figure S10: Experimental setup for the large-scale synthesis of Pd-NPs.

S7 Influence of mixing conditions on the NP size

It was found that the mixing conditions of precursor and $NaBH_4$ solution have an influence on the final size and size distribution of Pd-NPs. In this contribution, two techniques for the mixing of the reactants were used: A simple mixing with Eppendorf pipettes and a mixing applying peristaltic pump and Teflon mixer. In general, mixing with a pump and Teflon mixer is faster and more uniform than mixing with pipettes. Particles obtained from the fast and uniform mixing are smaller and have lower polydispersities than particles mixed with Eppendorf pipettes. Averaged mean radii and polydispersities in dependence of the mixing procedure are displayed in Table S4.

Table S4: Mean radii and polydispersity of Pd-NPs in dependence of the mixing conditions.

Mixing with Eppendorf pipettes		Mixing with pump and mixer	
r [nm]	poly [%]	r [nm]	poly [%]
2.3	30	2.1	25

S8 Evaluation of SAXS data

Mechanistic studies at lab scale were performed by use of a SAXS instrument (SAXSess, Anton Paar GmbH). The scattering curves of the colloidal solution were analyzed assuming spherical shape, a homogeneous electron density, and a Schulz-Zimm size distribution. The Schulz-Zimm distribution is given by:

$$f(r) = (z+1)^{z+1} x^2 \frac{\exp[-(z+1)x]]}{R_{avg}\Gamma(z+1)} \qquad (1)$$

where R_{avg} is the mean radius, $x = r/R_{avg}$, z is related to the polydispersity p ($p = \sigma/R_{avg}$) by $z = 1/p^2 - 1$, and σ^2 is the variance of the distribution. The scattering intensity of non-aggregated particles can be assumed to be proportional to the form factor of a single particle P(q). Thus, the scattering intensity of N monodisperse spheres with homogeneous electron density with volume V_{part} is given by:

$$I(q) = N \cdot I_{part}(q) = N \cdot V_{part}^2 P(q)$$

$$= N \cdot V_{part}^2 \cdot \left[\Delta\rho \frac{3(sin(qR) - qRcos(qR))}{qR}\right]^2 \qquad (2)$$

In case of polydisperse spherical particles one has to sum the scattering intensities over all particle sizes weighted by their frequency or to integrate using a size distribution function. It is common to use the Schulz-Zimm distribution for polydisperse particles. Hence, the scattering intensity is given by:

$$I(q) = N \int_0^\infty f(r)\, V_{part}^2 P(q) dr \qquad (3)$$

An analytical solution of the integral can be found in Kotlarchyk et al.[6] In order to analyze the nucleation and growth mechanism of nanoparticles, the number of particles is important. This information can be obtained by using the general relation of $I(q = 0)$ for a single particle, which is independent of its shape and size, i.e. $I = (\Delta\rho)^2 V^2$. Thus the scattered intensity $I(q = 0)$ of polydisperse particles can be written as

$$I(q = 0) = N\langle V^2\rangle\, (\Delta\rho)^2 \qquad (4)$$

where N is the number of particles and $\langle V^2\rangle$ the mean value of V^2. Due to the overlapping of the scattering intensity with the primary beam, $I(q = 0)$ cannot be measured directly, but is accessible *via* the extrapolation of $I(q)$ for $q \to 0$.

References

(1) Baes, C. F.; Mesmer, R. S. *Berichte Bunsenges. Für Phys. Chem.* **1977**, *81*, 245.
(2) Troitskii, S. Y.; Fedotov, M. A.; Likholobov, V. A. *Russ. Chem. Bull.* **1993**, *42*, 634.
(3) Simonov, P. A.; Troitskii, S. Y.; Likholobov, V. A. *Kinet. Catal.* **2000**, *41*, 255.
(4) Baylet, A.; Marécot, P.; Duprez, D.; Castellazzi, P.; Groppi, G.; Forzatti, P. *Phys. Chem. Chem. Phys.* **2011**, *13*, 4607.
(5) Polte, J.; Erler, R.; Thunemann, A. F.; Sokolov, S.; Ahner, T. T.; Rademann, K.; Emmerling, F.; Kraehnert, R. *Acs Nano* **2010**, *4*, 1076.
(6) Kotlarchyk, M.; Stephens, R. B.; Huang, J. S. *J. Phys. Chem.* **1988**, *92*, 1533.